

# Supplementary information for “The fate of aluminum in (Na,Bi)TiO<sub>3</sub>-based ionic conductors.”

Pedro B. Groszewicz<sup>a,c,†\*</sup>, Leonie Koch<sup>b,†\*</sup>, Sebastian Steiner<sup>c</sup>, Azatuhi Ayrikyan<sup>d</sup>, Kyle G. Webber<sup>d</sup>, Till Frömling<sup>c</sup>, Karsten Albe<sup>b\*</sup>, Gerd Buntkowsky<sup>a\*</sup>

a) Institute of Physical Chemistry, Technische Universität Darmstadt, Alarich-Weiss-Str. 8, D-64287 Darmstadt, Germany

b) Institute of Materials Science, Technische Universität Darmstadt, Otto-Berndt-Str. 3, D-64287 Darmstadt, Germany

c) Institute of Materials Science, Technische Universität Darmstadt, Alarich-Weiss-Str. 2, D-64287 Darmstadt, Germany

d) Department of Materials Science and Engineering, Friedrich-Alexander-Universität Martenstr. 5, D-91058 Erlangen, Germany

e) Present address: Department of Radiation Science and Technology, Delft University of Technology, Delft 2629JB, Netherlands

## Supporting Information

### Experimental Details to Materials Synthesis

Ceramic powders of all starting materials were produced by the solid oxide synthesis route. The oxide or carbonates of the respective elements, namely, Bi<sub>2</sub>O<sub>3</sub>, BaCO<sub>3</sub>, Al<sub>2</sub>O<sub>3</sub>, K<sub>2</sub>CO<sub>3</sub>, Na<sub>2</sub>CO<sub>3</sub>, and TiO<sub>2</sub> (all above 99.5% purity, Alfa Aesar GmbH & Co. KG, Karlsruhe, Germany), were mixed according to their stoichiometric formula and ball-milled in ethanol for 24 h. NKBT-6BA and NKBT-7BA were produced by calcination at 800 °C for 2 h, whereas NKBT-0.25BA was produced by calcination at 800 °C for 5 h. The samples were then shaped by uniaxial pressing and then isostatically pressed at 300MPa for 1.5 min. The NKBT-6BA and NKBT-7BA samples were sintered at 1100 °C for 2 h, with a 5 °C/min heating rate, while the NKBT-0.25BA samples were sintered at 1080 °C for 2 h. The acceptor-doped samples (e.g. NBT-xAl) were prepared in an analogous manner, with a stoichiometric amount of Al<sub>2</sub>O<sub>3</sub> substituting TiO<sub>2</sub> in the nominal composition of the powders (i.e. the Ti content was reduced to 1-x for x Al).

### Experimental Details to Impedance Spectroscopy

A Novocontrol Alpha A impedance analyzer was used to determine the frequency-dependent impedance. The frequency range of the probing signal was set between 0.1 Hz and 3 MHz with an amplitude of 0.1 V. The investigations were conducted at a 500 °C. For the analysis of the generated impedance results, the RelaxIS software was used.

### Experimental Details to NMR Measurements

Solid-state <sup>27</sup>Al NMR spectra were acquired with a Bruker Avance III spectrometer using a carrier frequency of 156.37 MHz. Ceramic pellets have been ground to powders. Successively, these powders have been mixed with boron nitride (1:2 volume) to facilitate spinning, which has been conducted under MAS conditions at a spinning frequency of 13 kHz and 14 kHz in 4 mm ZrO<sub>2</sub> rotors. For <sup>27</sup>Al MAS NMR experiments, a single-pulse sequence with a pulse length of 2.0 usec and a dwell time of 0.4 usec have ensured appropriate excitation and recording of the complete spectrum. A total number of 40960 scans have been accumulated with a recycle delay of 500 msec in between scans. No significant difference has been observed for longer recycle delays.

Two-dimensional <sup>27</sup>Al 3QMAS (or MQMAS) NMR spectra have been acquired with a Z-filter pulse sequence<sup>1</sup> with excitation, conversion, and Z-filter pulse durations of 4.3 usec, 1.5 usec, and 11.0 usec, respectively. The Z-filter delay has been 20 usec long, and 64 t<sub>1</sub> increments have been recorded in a rotor-synchronized fashion, with a recycle delay of 1.0 s and 3072 scans for each increment. The chemical shift scale was referenced to a 1 M AlCl<sub>3</sub> aqueous solution (0 ppm).

### Details to DFT Calculations

In the following study we will use the GIPAW formalism as implemented in the Vienna *Ab initio* Simulation Package (VASP)<sup>2-5</sup> by de Wijs et al.<sup>6</sup> For all calculations we used the generalized-gradient approximation (GGA) in the Perdew-Burke-Ernzerhof parameterization.<sup>7, 8</sup> We use a plane wave energy cut-off of 700 eV and chose a valence electron configuration of: O: 2s<sup>2</sup> 2p<sup>4</sup>, Na: 2p<sup>6</sup> 3s<sup>1</sup>, Ti: 3s<sup>2</sup> 3p<sup>6</sup> 4s<sup>2</sup> 3d<sup>2</sup>, Bi: 5d<sup>10</sup> 6s<sup>2</sup> 6p<sup>3</sup>, and Al: 3s<sup>2</sup> 3p<sup>1</sup>.

Sums on a  $\gamma$ -centered 3×3×3 k-point mesh have been used to approximate integrals over the Brillouin zone. For all following structural models with defined aluminum and oxygen vacancy arrangements, a cell composed of 160 atoms has been used.

The convergence of the calculated NMR values with respect to the energy cut-off and the k-point mesh has been carefully carried out, leading to an absolute maximum difference of around 0.1 ppm. This deviation is expected to be reasonable, considering the general spread found in the experimental and theoretical data.

The supercell size has been chosen such that the Al-substituents are sufficiently separated from their periodic images. Note that we initialized all calculations by using an optimized lattice constant instead of the experimental one. However, a calculation with a hydrostatically strained structure demonstrates that, despite small variations, the general trend remains valid. A more detailed description of the different structural motifs is given in the following sections.

Recent studies demonstrated that minimizing atomic forces prior to the actual calculation of the chemical shift is crucial for comparison with experiments and to serve as a tool for structural resolution under well controllable circumstances.<sup>9,10</sup> For this reason, atomic positions have been relaxed until atomic forces are below a threshold of 0.01 eV/Å for all cases studied. Moreover, we compare the influence of two different relaxation protocols. Firstly, we relaxed the atomic positions, while keeping the cell shape fixed. Secondly, we do not apply any constraint either on the atomic positions or on the cell shape. However, the volume remains constant in both approaches.

### <sup>27</sup>Al MAS NMR spectrum of NKBT-7BA - satellite transitions

Complete MAS NMR spectrum of NKBT-7BA showing the satellite transitions. The shape of the spinning sidebands envelope (SSE) indicates a distribution of quadrupolar coupling constants ( $C_Q$ ) for the main aluminum site in NKBT-7BA. Based on its width, a  $C_Q$  value around 2 MHz can be estimated for this  $Al^{3+}$  site, which matches the value of  $C_Q$  estimated from the quadrupolar induced shift of the main signal in the <sup>27</sup>Al 3QMAS spectrum of this sample. Furthermore, simulations of the satellites for a distribution of  $C_Q$  values about  $C_Q=2$  MHz further supports this value. For comparison, the simulation of the satellites for a single  $C_Q$  value of 2 MHz is also displayed. Simulations of these 1D spectra were calculated with SIMPSON.<sup>11</sup>

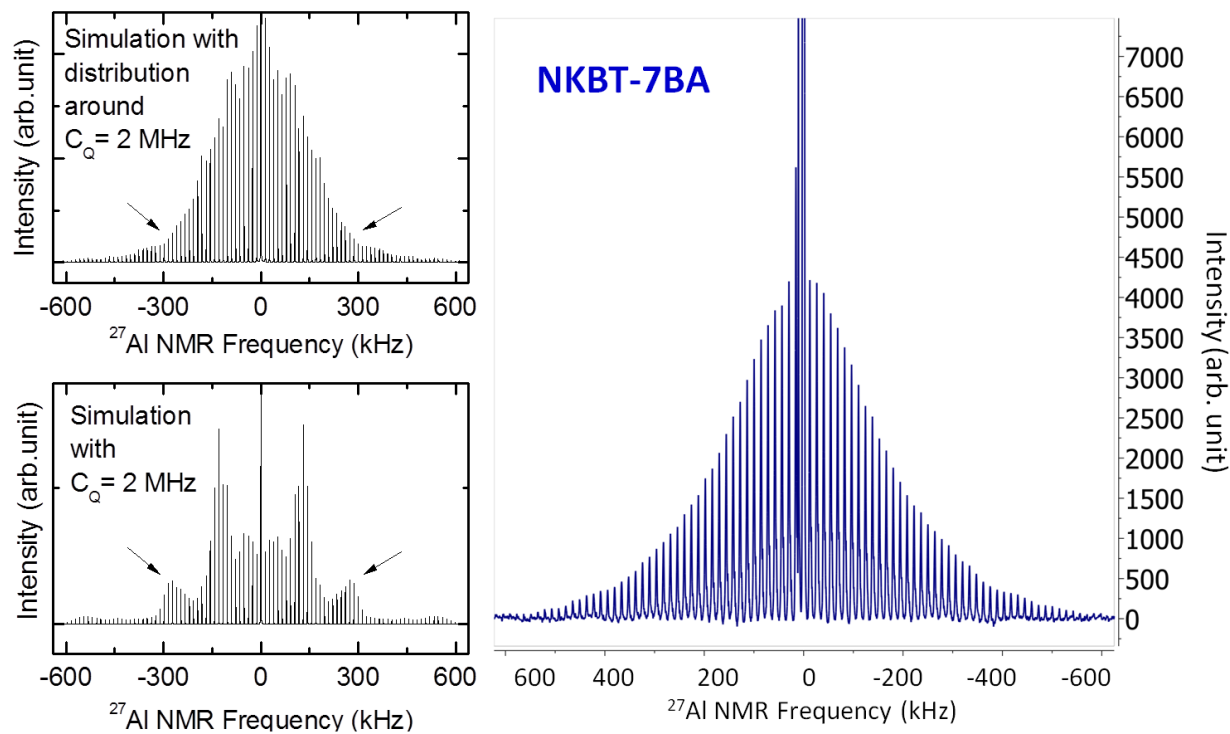


**Figure S1:** Spinning sidebands envelope of <sup>27</sup>Al satellite transitions. (MAS 13 kHz) Right: Focus on BNKT-7BA, detail on the kink both sides 300 kHz away from the central transition. Left: Simulations for a <sup>27</sup>Al spectrum with  $C_Q=2$  MHz. Top: distribution of  $C_Q$  values. Bottom: single site with  $C_Q=2$  MHz.

**$^{27}\text{Al}$  3QMAS NMR spectra of NBT-4Al, NKBT-6BA and NKBT-7BA**

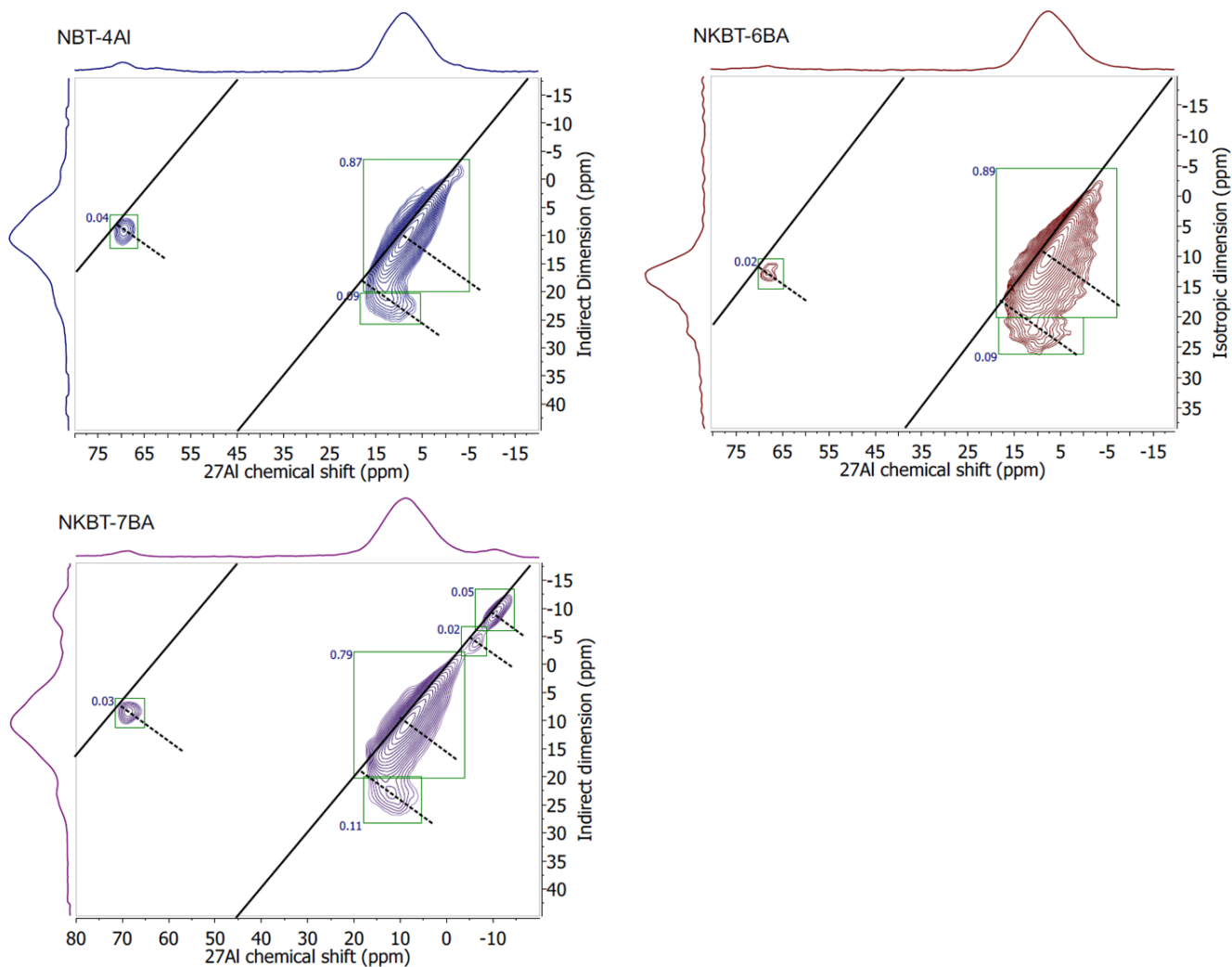


**Figure S2:** Additional  $^{27}\text{Al}$  3QMAS NMR spectra, displayed with projections on the MAS and indirect dimensions. The isotropic line is depicted as a black diagonal line, which is aliased as a consequence of the spectral window in the indirect dimension. All spectra have in common a broad signal at 9 ppm, attributed to aluminum at the regular B-site. In addition to that, all spectra exhibit a second resonance in the  $\text{AlO}_6$  range and a resonance in the  $\text{AlO}_4$ , which are both assigned to a secondary phase, due to its similarity to the spectrum of  $\text{Bi}_2\text{Al}_4\text{O}_9$ .

$^{27}\text{Al}$  3QMAS NMR spectrum of  $\text{Bi}_2\text{Al}_4\text{O}_9$

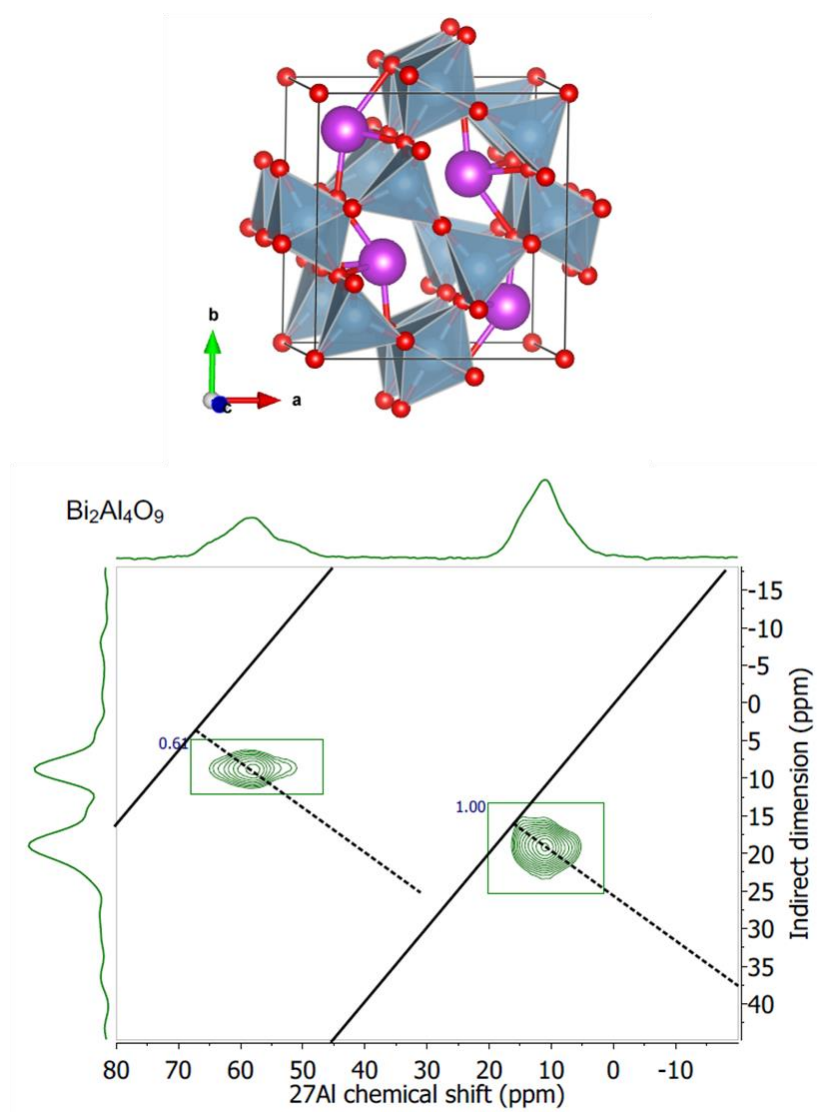


**Figure S3:** Top: Unit cell of  $\text{Bi}_2\text{Al}_4\text{O}_9$  exhibiting both  $\text{AlO}_6$  and  $\text{AlO}_4$  sites. Bottom  $^{27}\text{Al}$  3QMAS NMR spectra of  $\text{Bi}_2\text{Al}_4\text{O}_9$ , for which the signals of each site are well resolved, both in the MAS and the indirect dimension.

### Comparison between Impedance spectroscopy and $^{27}\text{Al}$ MAS NMR spectra of NBT-0.5Al, NBT-0.3Al and NBT-0.1Al

The comparison of NBT- $x$ Al samples in the low concentration range of acceptor doping further highlights the relation between the low sample impedance (Figure S4) and the absence of a pentacoordinated aluminum sites (Figure S5). In this way, the high ionic conductivity of samples NBT-0.5Al and NBT-0.3Al is interpreted as a consequence of disassociated vacancies. This behavior is in stark contrast to sample NBT-0.1Al, where Al- $\text{V}_\text{O}^{**}$  associated defects are present.

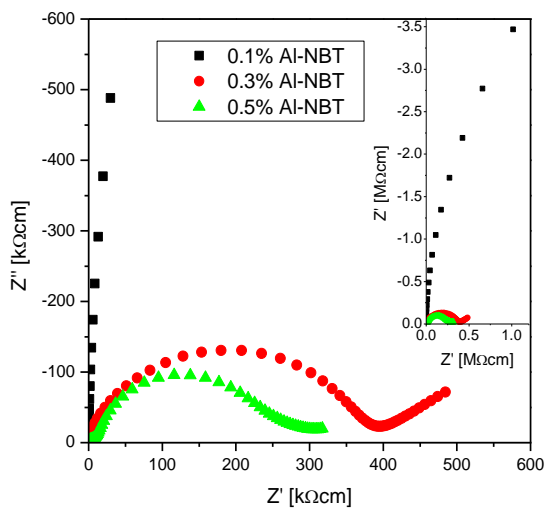


Figure S4: Impedance spectra of Al-doped NBT compositions with different Al concentrations at 500°C.

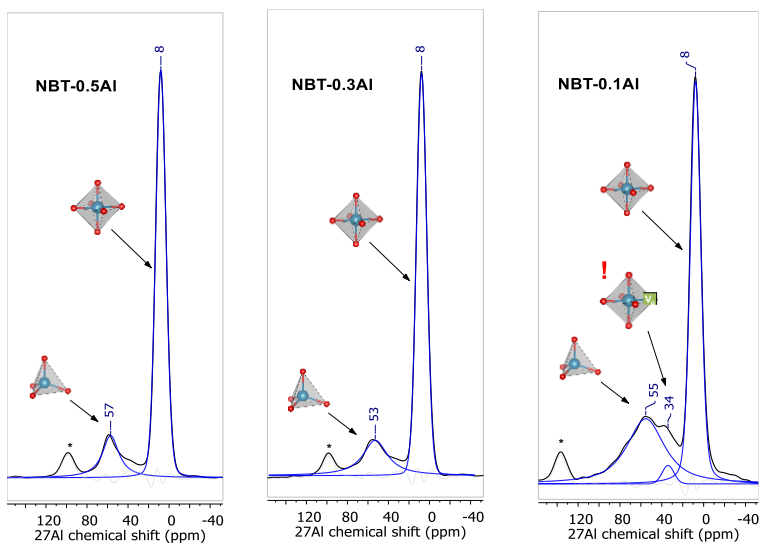


Figure S5:  $^{27}\text{Al}$  MAS NMR spectra of Al acceptor doped NBT- $x$ Al. Spinning frequencies of 14 kHz and 13 kHz have been used, respectively.

## Arrhenius plot for NBT-Al compositions

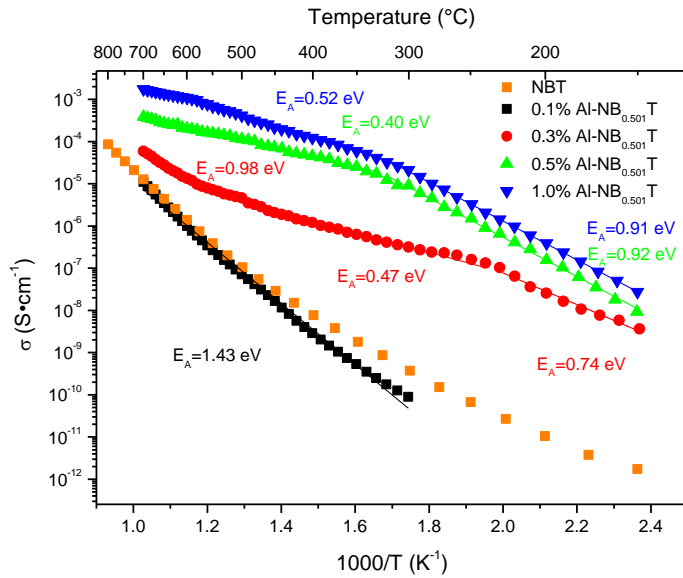


Figure S6: Arrhenius plot for the bulk conductivity  $\sigma$  of Al-doped NBT compositions with varying doping contents.

## Impedance Spectroscopy for NKBT-BA compositions

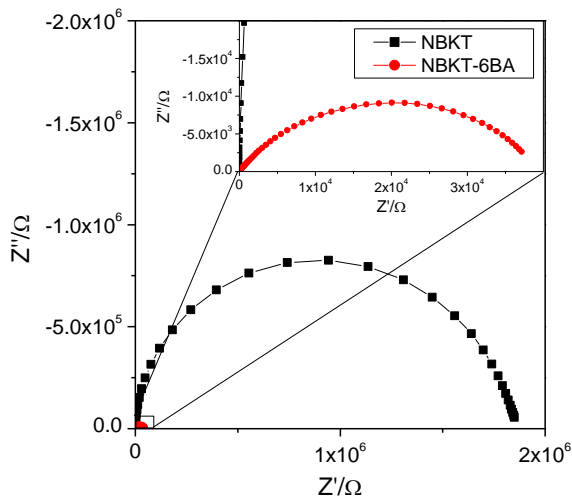


Figure S7: Impedance spectra of NKBT compositions with and without  $\text{BiAlO}_3$  solid-solution, measured at  $500^\circ\text{C}$ .

## AUTHOR INFORMATION

### Corresponding Author

\*Pedro B. Groszewicz, ORCID: 0000-0002-5246-6449

eMail: [groszewicz@chemie.tu-darmstadt.de](mailto:groszewicz@chemie.tu-darmstadt.de);

\*Leonie Koch,

eMail: [koch@mm.tu-darmstadt.de](mailto:koch@mm.tu-darmstadt.de);

\*Karsten Albe, ORCID: 0000-0003-4669-8056

eMail: [albe@mm.tu-darmstadt.de](mailto:albe@mm.tu-darmstadt.de);

\*Gerd Buntkowsky, ORCID: 0000-0003-1304-9762

eMail: [gerd.buntkowsky@chemie.tu-darmstadt.de](mailto:gerd.buntkowsky@chemie.tu-darmstadt.de)

### Author Contributions

‡These authors contributed equally.

## Notes

The authors declare no competing financial interests.

## ACKNOWLEDGMENT

The authors gratefully acknowledge financial support by the Deutsche Forschungsgemeinschaft (DFG) through project Grants No. AL 578/20-1, No. BU 911/28-1, No. WE 4972/5 and No. FR 3718/1-1. Computing time was granted by the John von Neumann Institute for Computing (NIC) and provided on the supercomputer JURECA at Jülich Supercomputing Centre (JSC). Additional calculations for this research were conducted on the Lichtenberg high performance computer of the TU Darmstadt. The authors would like to thank An-Phuc Hoang for the assistance of preparing doped samples.

## REFERENCES

1. Amoureux, J.-P.; Fernandez, C.; Steuernagel, S., *J Magn. Reson. A* **1996**, 123, (1), 116-118.
2. Kresse, G.; Hafner, J., *Phys. Rev. B* **1994**, 49, (20), 14251–14269.
3. Kresse, G., *J. Non-Cryst. Solids* **1995**, 192-193, 222–229.
4. Kresse, G.; Furthmüller, J., *Comput. Mater. Sci.* **1996**, 6, (1), 15–50.
5. Kresse, G.; Furthmüller, J., *Phys. Rev. B* **1996**, 54, (16), 11169–11186.
6. de Wijs, G. A.; Laskowski, R.; Blaha, P.; Havenith, R. W. A.; Kresse, G.; Marsman, M., *J. Chem. Phys.* **2017**, 146, (6), 064115.
7. Perdew, J. P.; Burke, K.; Ernzerhof, M., *Phys. Rev. Lett.* **1996**, 77, (18), 3865–3868.
8. Perdew, J. P.; Burke, K.; Ernzerhof, M., *Phys. Rev. Lett.* **1997**, 78, (7), 1396.
9. Yates, J. R.; Pickard, C. J.; Mauri, F., *Phys. Rev. B* **2007**, 76, 024401.
10. Ashbrook, S. E.; McKay, D., *Chem. Commun.* **2016**, 52, 7186–7204.
11. Bak, M.; Rasmussen, J. T.; Nielsen, N. C., *J.Magn.Res.* **2000**, 147, 296.